

1 SARS-CoV-2 Infects Syncytiotrophoblast and Activates
2 Inflammatory Responses in the Placenta
3

4
5 Lissenya B. Argueta^{1,*}, Lauretta A. Lacko^{2,*}, Yaron Bram^{3,*}, Takuya Tada⁴, Lucia
6 Carrau⁵, Tuo Zhang⁶, Skyler Uhl⁵, Brienne C. Lubor¹, Vasuretha Chandar³, Cristianel
7 Gil², Wei Zhang⁶, Brittany Dodson⁷, Jeroen Bastiaans¹, Malavika Prabhu⁷, Christine M.
8 Salvatore⁹, Yawei J. Yang^{7,8}, Rebecca N. Baergen⁸, Benjamin R. tenOever⁵, Nathaniel
9 R. Landau⁴, Shuibing Chen^{2,#}, Robert E. Schwartz^{3,#}, Heidi Stuhlmann^{1,10,#}

10
11 Department of Cell and Developmental Biology, Weill Cornell Medicine, 1300 York
12 Avenue, New York 10065, NY, USA¹

13 Department of Surgery, Weill Cornell Medicine, New York, NY, USA²

14 Division of Gastroenterology and Hepatology, Department of Medicine, Weill Cornell
15 Medicine, New York, NY, USA³

16 Department of Microbiology, NYU Grossman School of Medicine, New York, NY, USA⁴

17 Department of Microbiology, Icahn School of Medicine at Mount Sinai, New York, NY,
18 USA⁵

19 Genomics Resources Facility, Weill Cornell Medicine, New York, NY, USA⁶

20 Department of Obstetrics and Gynecology, Weill Cornell Medicine, New York, NY, USA⁷

21 Department of Pathology and Laboratory Medicine, Weill Cornell Medicine, New York,
22 NY, USA⁸

23 Department of Pediatrics, Division of Pediatric Infectious Diseases, Weill Cornell
24 Medicine, New York, NY, USA⁹

25 Department of Pediatrics, Weill Cornell Medicine, New York, NY, USA¹⁰

26

27

28 *These authors contributed equally

29

30 #Corresponding Authors:

31 Heidi Stuhlmann PhD (lead contact) hes2011@med.cornell.edu

32 Robert Schwartz MD-PhD res2025@med.cornell.edu

33 Shuibing Chen PhD shc2034@med.cornell.edu

34

35 **Abstract**

36 SARS-CoV-2 infection during pregnancy leads to an increased risk of adverse
37 pregnancy outcomes. Although the placenta itself can be a target of virus infection,
38 most neonates are virus free and are born healthy or recover quickly. Here, we
39 investigated the impact of SARS-CoV-2 infection on the placenta from a cohort of
40 women who were infected late during pregnancy and had tested positive for SARS-
41 CoV-2 by qRT-PCR at delivery. SARS-CoV-2 genomic and subgenomic RNA was
42 detected in 23 out of 55 placentas (41%). Three placentas with high virus content were
43 obtained from mothers who presented with severe COVID-19 and whose pregnancies
44 resulted in adverse outcomes for the fetuses, including intrauterine fetal demise,
45 stillbirth, and a preterm delivered baby still in newborn intensive care. Examination of
46 the placental samples with high virus content showed efficient SARS-CoV-2 infection,
47 using RNA in situ hybridization to detect genomic and replicating viral RNA, and
48 immunohistochemistry to detect SARS-CoV-2 nucleocapsid protein. Infection was
49 restricted to syncytiotrophoblast cells that envelope the fetal chorionic villi and are in
50 direct contact with maternal blood. The infected placentas displayed massive infiltration
51 of maternal immune cells including macrophages into intervillous spaces, potentially
52 contributing to inflammation of the tissue. *Ex vivo* infection of placental cultures with
53 SARS-CoV-2 or with SARS-CoV-2 spike (S) protein pseudotyped lentivirus targeted
54 mostly syncytiotrophoblast and, to a lesser extent, endothelial cells. Infection was
55 reduced by using blocking antibodies against ACE2 and against Neuropilin 1,
56 suggesting that SARS-CoV-2 may utilize alternative receptors for entry into placental
57 cells.

58 **Introduction**

59 The global pandemic resulting from the novel coronavirus, Severe acute respiratory
60 syndrome coronavirus 2 (SARS-CoV-2), has already taken a devastating toll, with over
61 170 million total cases and more than 3.5 million deaths worldwide. SARS-CoV-2 which
62 causes Coronavirus Disease 2019 (COVID-19) has significant clinical variability. In
63 severe cases SARS-CoV-2 causes the respiratory illness, whose defining features are
64 an imbalanced inflammatory host response, reduced innate antiviral defenses and an
65 inflammatory “cytokine storm”, endothelial damage, coagulopathies and thrombosis in
66 several tissues from infected patients (Blanco-Melo et al. 2020).

67 To date, our understanding of how SARS-CoV-2 infection impacts pregnancy,
68 including the health of COVID-19 positive mothers and their babies, remains
69 incomplete. Pregnant women with symptomatic COVID-19 infections are more likely to
70 be admitted to the intensive care unit (ICU), and have statistically higher maternal death
71 rates when compared to non-pregnant infected women (Zambrano et al. 2020). While
72 preterm deliveries occur more often in women with suspected or confirmed SARS-CoV-
73 2 infection, no increase in stillbirth or early neonatal death was found (Mullins et al.
74 2021). Prospective and retrospective studies showed that pregnant women infected with
75 SARS-CoV-2 are at increased risk of adverse events, including higher rates of cesarean
76 section and increased post-partum complications (Woodworth et al. 2020; Prabhu et al.
77 2020; Marín Gabriel et al. 2020). While vertical transmission of SARS-CoV-2 from
78 mother to fetus has been reported in a few cases (Hecht et al. 2020a; Vivanti et al.
79 2020; Taglauer et al. 2020; Facchetti et al. 2020; Woodworth et al. 2020; Hecht et al.
80 2020b; Alamar et al. 2020), most studies did not detect viral transmission (Penfield et al.

81 2020; Baergen and Heller 2020; Prabhu et al. 2020; Salvatore et al. 2020; Edlow et al.
82 2020; Schwartz 2020; Della Gatta et al. 2020; Kimberlin and Stagno 2020).

83 Several studies have detected SARS-CoV-2 infection of the placentas from women
84 who tested positive for the virus at, or prior to, delivery. In some cases, the placenta
85 displayed signs of inflammation. These placentas were found to have increased
86 vascular malperfusion indicative of thrombi in fetal vessels (Baergen and Heller 2020;
87 Vivanti et al. 2020; Prabhu et al. 2020; Shanes et al. 2020) and infiltration of maternal
88 immune cells (Hosier et al. 2020; Facchetti et al. 2020; Debelenko et al. 2021; Garrido-
89 Pontnou et al. 2021; Lu-Culligan et al. 2021; Morotti et al. 2021; Schwartz et al. 2021).

90 Whether inflammation results from virus infection of the mother or direct infection of the
91 placenta remains unresolved, as this may depend on the gestational age of the fetus.
92 Virus infection is known to impair placental function. Virus-associated inflammation
93 during pregnancy can result in chronic cardiovascular disease, diabetes and obesity
94 later in life (Burton, Fowden, and Thornburg 2016). Little is known however about the
95 effect of SARS-CoV-2 placental function.

96 SARS-CoV-2 utilizes ACE2 (Angiotensin-converting enzyme 2) as the primary
97 receptor (Hoffmann et al. 2020), and Neuropilin-1 (NRP1) as a coreceptor (Cantuti-
98 Castelvetro et al. 2020; Daly et al. 2020), in concert with the two proteinases TMPRSS2
99 (Transmembrane protease serine 2) (Hoffmann et al. 2020) and CTSL (Ou et al. 2020)
100 and the pro-protein convertase furin (Shang et al. 2020), amongst others (Wei et al.
101 2021; Daniloski et al. 2021; Wang et al. 2021; Schneider et al. 2021) for cell entry. All of
102 the viral entry receptors are expressed at significant levels in first and second trimester
103 placentas. However, at term they are expressed at lower levels at the maternal-fetal

104 interface, including the placenta and the chorioamniotic membranes (Pique-Regi et al.
105 2020; Li et al. 2020; Singh, Bansal, and Feschotte 2020; Taglauer et al. 2020; Lu-
106 Culligan et al. 2021; Baston-Buest et al. 2011). Whether alternative entry mechanisms
107 are exploited by SARS-CoV-2 in the placenta is not known.

108 In this study we were interested to understand the impact of SARS-CoV-2 infection
109 late in pregnancy on placental function. Using a cohort of 55 women who tested positive
110 for SARS-CoV-2 at the time of delivery, we report on placental infections, placental
111 pathologies and *in vivo* inflammatory responses to infection. Furthermore, we present *in*
112 *situ* studies of infected placentas as well as *ex vivo* placental explant cultures that
113 investigate susceptibility of placental cells to SARS-CoV-2 infection.

114

115 **Results**

116 **Clinical presentations of SARS-CoV-2 positive mothers, fetal outcomes and**
117 **placental pathologies**

118 A cohort of 55 women who were identified as positive for SARS-CoV-2 by RT-PCR
119 from nasopharyngeal swabs at the time of admission for delivery at NY Presbyterian
120 Hospital-Weill Cornell was included in the present study (P1–P55). As controls, a
121 cohort of 5 women who tested negative for SARS-CoV-2 (C1-C5), and a cohort of 5
122 SARS-CoV-2 negative women who presented various placental inflammatory
123 pathologies (I1-I5) were also included in the study (Table 1).

124 The pregnant women ranged in age from 16 to 51 years, with a majority in their 20's
125 and 30's. Among the 55 women who tested positive for SARS-CoV-2, 10 were
126 symptomatic for COVID-19 (18%), and several presented additional comorbidities
127 including hypertension, diabetes, and obesity. None of the women required intensive
128 care. Four pregnancies resulted in intrauterine fetal demise (IUFD) or stillbirth (P2, P3,
129 P7, P38), and one of the four (P38) presented with anencephaly. One fetus, delivered
130 preterm at 25 weeks of gestation, was admitted to the neonatal intensive care unit
131 (NICU), where the infant has remained for 4 months (P1). All other neonates, including
132 3 sets of twins, had normal Apgar scores at 1 min and at 5 min after birth and were
133 healthy at initial follow up (Table 1). All neonates were tested by nasopharyngeal swabs
134 for SARS-CoV-2 at 24 hours, and none were positive. Among the placentas delivered
135 from mothers who tested positive for SARS-CoV-2, 30% (17 cases) presented fetal
136 vascular malperfusion (FVM), 18% (10 cases) displayed maternal vascular malperfusion
137 (MVM), and 7% (4 cases) overlapped for both placental pathologies. None of the

138 healthy control placentas from SARS-CoV-2 negative mothers displayed FVM or MVM
139 (Table 1).

140 RNA was isolated from all placental samples and subjected qRT-PCR to determine
141 the presence of genomic and replicating SARS-CoV-2 RNA. 23 out of 55 placentas from
142 SARS-CoV-2 positive mothers showed presence of viral RNA (42%), 3 of those were
143 highly positive (5%), 10 positive (18%) and 10 were borderline positive (18%) (Table 1
144 and Figure 1A). Presence of SARS-CoV-2 in the placenta did not correlate with
145 observed FVM: Of the 23 positive placentas, 10 displayed FVM while 13 were without
146 FVM (Table 1).

147 Strikingly, all four pregnancies from SARS-CoV-2 positive mothers that resulted in
148 IUD, stillbirth or admission of the neonate to the NICU, delivered placentas that were
149 highly positive (P1-P3) or positive (P7) for SARS-CoV-2 (Table 1, grey shaded rows).
150 Conversely, all other pregnancies from SARS-CoV-2-positive mothers resulted in the
151 delivery of healthy neonates, with the exception of one case with anencephaly (P38).

152

153 **Placental syncytiotrophoblast are the primary target for SARS-CoV-2 infection of
154 pregnant females at term**

155 To determine whether the placenta itself was infected by SARS-CoV-2, qRT-PCR
156 using primers against SARS-CoV-2-N was run on RNA isolated from FFPE patient
157 placenta slides. This provided us with 5 distinct cohorts for this study depicted in Table
158 1: High Positive (P1-P3; ddCT value > 9), Positive (P4-P13; ddCT > 4.5), and Borderline
159 Positive (P14-P23). We also ran qRT-PCR on RNA from patient placenta samples from
160 SARS-CoV-2 negative mothers (C1-C5) as well as SARS-CoV-2 negative mothers that

161 had unrelated inflammatory pathologies (I1-I5) (Figure 1A and Table 1). To confirm
162 presence of viral RNA, the presence of a distinct amplicon on PCR melt curve and on
163 gels run on RNA samples distinguished between the positive and negative samples
164 from all of the placenta samples obtained from COVID-positive mothers (data not
165 shown).

166 To identify the cells in the placental chorionic villi that were infected by SARS-CoV-2,
167 adjacent placental sample sections (10 microns apart) from the different cohorts were
168 stained by hematoxylin and eosin (H&E), or for the presence of replicating viral RNA, for
169 the presence of SARS-CoV-2 nucleocapsid protein (SARS-CoV-2-N), and for the
170 presence CD163⁺ Hofbauer cells (HBC) and macrophages using
171 immunohistochemistry. SARS-CoV-2 RNA was detected by *in situ* hybridization in the
172 high positive samples, but not in negative control samples (Figure 1B). Presence of
173 SARS-CoV-2 RNA was restricted to the Keratin-7 (KRT7)-positive syncytial trophoblast
174 layer which anatomically encapsulate the chorionic villi structures (Figure 1B). Similarly,
175 expression of the SARS-CoV-2 N protein was detected in adjacent sections within the
176 same villi. Localization of the N protein was restricted to the syncytiotrophoblast layers
177 in the high positive placentas. Interestingly, the syncytial trophoblast layer of the high
178 positive sample had significantly fewer nuclei and appeared damaged as indicated by
179 the hematoxylin counterstaining. Importantly, at low magnification, massive infiltration of
180 maternal immune cells, including CD163+ macrophages detected in the high positive
181 samples, but not in the controls (Figure 1B and not shown). This result is consistent with
182 the pathology report for the sample P3 of chronic histiocytic intervillousitis (CHI) (Table
183 1). Intravillous HBC and intervillous maternal macrophages did not show infection with

184 SARS-CoV-2, evidenced by the absence of SARS-CoV-2 RNA and N protein. In
185 summary, these results indicate that syncytiotrophoblast are the primary targets for
186 SARS-CoV-2 infection in the placenta, and that the massive maternal immune cell
187 migration occurred in response to the SARS-CoV-2 infection either in the mother or in
188 the placenta.

189

190 **Placental explant and cell cluster cultures are permissive to pseudo-entry virus**
191 **and infection can be blocked by anti-ACE2 and anti-NRP1 antibodies**

192 To determine the SARS-CoV-2 tropism and infection of term placentas, we used
193 fresh placental isolates from SARS-CoV-2 negative mothers obtained immediately post-
194 delivery. After removal of the fetal chorionic plate and maternal decidua, samples
195 containing terminal, intermediate and stem chorionic villi were used for the preparation
196 of placental villi explant cultures (Figure 2C). In addition, placental cell clusters were
197 prepared by enzymatic digestion of the chorionic villi, followed by filtration that allows
198 passage of small cell clusters. Placental cultures were infected with a dual
199 nanoluciferase/green fluorescent protein (GFP) reporter lentiviral vector pseudotyped
200 with SARS-CoV-2 spike (S) (Tada et al. 2020), and luciferase activity was quantified 72
201 hpi. Lentiviral reporter viruses pseudotyped with vesicular stomatitis virus G protein
202 (VSV-G) were used as a positive control for infection (Figure 2). A comparison of the
203 infectivity showed that both pseudotyped viruses infected the placental cultures at
204 similar levels. Explant cultures consistently showed an approximately 5-fold lower
205 infection as compared to clusters or single cells, likely due to the reduced surface
206 accessibility. Infectivity was significantly reduced by adding the human

207 immunodeficiency virus (HIV) reverse transcriptase (RT) inhibitor nevirapine (NVP),
208 indicating that the luciferase activity was primarily due to viral entry and not carry-over
209 from residual viral particles in the cultures (Figure 2A). The major SARS-CoV-2 entry
210 factors, ACE2 and TMPRSS2 are expressed in the placenta, albeit their expression is
211 significantly decreased in the third trimester (Pique-Regi et al. 2020; Singh, Bansal, and
212 Feschotte 2020; Ouyang et al. 2021). Furthermore, NRP1 has been identified as a
213 novel host factor for SARS-CoV-2 (Cantuti-Castelvetro et al. 2020; Daly et al. 2020) and
214 is expressed on syncytiotrophoblast (Arad et al. 2017; Baston-Buest et al. 2011). To
215 determine if ACE2 and/or NRP1 facilitate infection in the placenta, we pre-treated
216 placental cell clusters with anti-ACE2 or anti-NRP1 blocking antibody prior to infection.
217 Both antibodies reduced infectivity of SARS-CoV-2 S protein pseudotyped lentivirus in
218 placental cell clusters by about 50%, while anti-ACE2 blocking antibody did not reduce
219 infectivity of VSV-G pseudotyped lentivirus. Pre-treatment with both antibodies did not
220 result in further reduction of infectivity, suggesting the possibility of alternative
221 receptor(s) (Figure 2B).

222 To determine which cells are targeted by the pseudotyped virus, placental explant
223 cultures were infected for 72 hours with lentivirus pseudotyped by SARS-CoV-2 spike
224 (S) protein, and live GFP could be visualized in the infected explant cultures, with a
225 more robust signal observed in the pseudotyped VSV-G infected cultures (Figure 2C).
226 Explant cultures were then processed for immunofluorescence staining and analyzed
227 for co-localization of the GFP reporter with KRT-7/Cytokeratin (trophoblast marker) and
228 CD31 (endothelial marker). GFP was detected in small patches of syncytiotrophoblast
229 cells located on the outer perimeter of the chorionic villi, but not in endothelial cells

230 (Figure 2D). Similar results were obtained after infection with VSV-G pseudotyped
231 lentivirus, with more robust infection visualized by live fluorescence microscopy on the
232 infected explant cultures, whereas no GFP signal was found in mock-infected explant
233 cultures (Figure 2D).

234

235 **Primary placental cell clusters are permissive to SARS-CoV-2**

236 To further determine the intrinsic susceptibility of placental cells to SARS-CoV-2,
237 primary placental cell clusters were infected *ex vivo*. Placentas were isolated from
238 healthy term deliveries as described above, digested into cell clusters of approximately
239 50-100 cells and plated on Matrigel-coated plates. Cell clusters were infected with live
240 SARS-CoV-2 virus (Isolate USA-WA1/2020, multiplicity of infection, MOI=1). Cells were
241 collected 24 hpi and virus load analyzed by qRT-PCR and immunofluorescence
242 staining.

243 qRT-PCR analysis using primers targeting subgenomic N transcripts demonstrated
244 robust SARS-CoV-2 viral replication in primary human placental cell clusters at 24 hpi
245 (Figure 3A). To determine which cells of primary placental cell clusters were susceptible
246 to SARS-CoV-2 infection, infected cell clusters were immunostained for SARS-CoV-2
247 nucleocapsid protein (SARS-N) and cell type specific markers for trophoblast cells
248 (KRT7) and endothelial cells (CD31). Three-dimensional reconstruction of confocal
249 imaging confirmed the presence of SARS-CoV-2-N protein in KRT7+
250 syncytiotrophoblast (Figure 3B). Co-localization of SARS-CoV-2-N protein was found in
251 multiple clusters of KRT7+ syncytiotrophoblast cells (Figure 3C). In addition to the

252 positive staining for SARS-CoV-2-N in syncytiotrophoblast, there were rare CD31+
253 endothelial cells that also stained positively for SARS-CoV-2-N protein (Figure 3C).

254

255 **Discussion**

256 The placenta is a vital organ that provides the gestational interface between mother
257 and fetus. Compromised maternal health and environmental insults, such as viral
258 infections, can result in placental dysfunction and lead to pregnancy complications with
259 increased morbidity and mortality for the mother and fetus (Rossant and Cross 2001;
260 Maltepe, Bakardjiev, and Fisher 2010; John and Hemberger 2012). Impairment of
261 placental function can also developmentally program the fetus for chronic disease later
262 in life, including cardiovascular disease, diabetes and obesity (Burton, Fowden, and
263 Thornburg 2016).

264 The aim of our study was to investigate the impact of late pregnancy SARS-CoV-2
265 infection on maternal and fetal health and proper placental function. Within a cohort of
266 56 placental samples from women who tested positive for SARS-CoV-2 at delivery, 23
267 were positive for genomic and replicating viral RNA. The observed percentage of
268 positive samples was higher compared to other studies (Hecht et al. 2020b; Facchetti et
269 al. 2020; Debelenko et al. 2021; Lu-Culligan et al. 2021) and likely reflects the fact that
270 New York City was at the epicenter for COVID-16 in May-May of 2020. Furthermore,
271 many of the placental samples were obtained from deliveries where the mothers or
272 infants presented with clinical pathologies. Importantly, quantification of virus content in
273 the placental samples allowed us for the first time to uncover a striking correlation in 3
274 out of 3 cases between symptomatic COVID-19 of the mother at the time of delivery,
275 high SARS-CoV-2 presence in the placenta, and adverse fetal outcome, including fetal
276 demise and preterm delivery. In contrast, only 1 out of 10 pregnancies with medium viral
277 content resulted in intrauterine fetal demise, and this may have been triggered by poorly

278 controlled maternal T2D. Of the pregnancies with medium or low virus content in the
279 placenta, all 18 babies tested negative for SARS-CoV-2 and were healthy at discharge.
280 It will be important to follow up on the health of these infants to investigate possible
281 long-term effects of SARS-CoV-2. None of the pregnancies of SARS-CoV-2 negative
282 healthy controls (n=5) or inflammation controls (n=5) resulted in fetal demise.

283 Upon examining sections from placentas with high virus content, we detected SARS-
284 CoV-2 RNA and protein in a large fraction of syncytiotrophoblast, the single cell layer
285 enveloping the fetal chorionic villi situated at the interphase to maternal blood. No virus
286 was detected in fetal macrophages (Hofbauer cells), other cell types inside the villi,
287 including stromal and endothelial cells, or outside the villi. Several recent reports also
288 provided evidence for SARS-CoV-2 infection restricted to syncytiotrophoblast of
289 placentas from SARS-CoV-2 positive mothers (Alamar et al. 2020; Mulvey et al. 2020;
290 Hecht et al. 2020b; Penfield et al. 2020; Hosier et al. 2020; Vivanti et al. 2020; Taglauer
291 et al. 2020; Facchetti et al. 2020). However, two reports on a preterm placenta and a
292 placenta from a newborn with vertically SARS-CoV-2 noted also presence of SARS-
293 CoV-2 in other cell types, including Hofbauer cells and stromal cells inside the villi, and
294 maternal macrophages and epithelial cells at the maternal-fetal interface (Verma et al.,
295 2021, Fachetti et al, 2020). It is possible that SARS-CoV-2 infection in these cases
296 occurred at earlier gestational stages and allowed for additional viral spread beyond the
297 syncytiotrophoblast layer.

298 Placentas in our study with high virus presence also displayed massive infiltration of
299 maternal immune cells, including macrophages into the intervillous space. However, we
300 did not detect SARS-CoV-2 in the infiltrating immune cells. Several recent studies

301 reported similar findings; interestingly they were most prominently found in placentas
302 from live-borne and stillborn neonates that had tested positive for SARS-CoV-2. These
303 finding included intervillous infiltration by inflammatory immune cells, chronic histiocytic
304 intervillitis with trophoblast necrosis, and increased fibrin deposition (Debelenko et al.
305 2021; Facchetti et al. 2020; Garrido-Pontnou et al. 2021; Lu-Culligan et al. 2021;
306 Schwartz et al. 2021; Morotti et al. 2021; Verma et al. 2021). Furthermore,
307 transcriptome data presented in one of these studies showed localized inflammatory
308 responses to systemic SARS-CoV-2 infection in the placenta, even if SARS-CoV-2 virus
309 was not detected (Lu-Culligan et al. 2021).

310 Considering the low efficiency of placental infection by SARS-CoV-2, we decided to
311 complement our *in vivo* studies by using *ex vivo* placental explant and cell cluster
312 culture models to study virus entry. We showed infection with SARS-CoV-2 virus or
313 SARS-CoV-2 spike S pseudotyped lentivirus targeted predominantly
314 syncytiotrophoblast and, in rare instances, endothelial cells. Term placentas express
315 very low levels of the SARS-CoV-2 receptor ACE2 and the co-factor TMPRSS2 (Pique-
316 Regi et al. 2020; Singh, Bansal, and Feschotte 2020; Ouyang et al. 2021). Recently, Lu-
317 Culligan et al. (Lu-Culligan et al. 2021) reported on increased levels of placental ACE2
318 expression in COVID-19 positive mothers; whereas a second publication reported on a
319 decrease of ACE2 expression and dysregulation of the renin-angiotensin system
320 (Verma et al. 2021). We asked here if alternative entry factors might be used by SARS-
321 CoV-2 to infect placental cells. One likely candidate is the transmembrane protein
322 NRP1, which has recently been identified as a host factor that facilitates SARS-CoV-2
323 cell entry and infectivity (Cantuti-Castelvetro et al. 2020; Daly et al. 2020). NRP1 was

324 originally identified as a co-receptor for Vascular endothelial growth factor (VEGF) on
325 endothelial cells but is expressed also at the maternal-fetal interface in decidual cells
326 and syncytiotrophoblast, and is thought to play important roles during pregnancy and in
327 the immune system (Arad et al. 2017; Baston-Buest et al. 2011). We show that infection
328 by SARS-CoV-2 S pseudotyped lentivirus can be partially inhibited by using blocking
329 anti-ACE2 or anti-NRP1 antibodies, whereas infection by VSV-G pseudotyped lentivirus
330 is not blocked, suggesting that SARS-CoV-2 may use NRP1 as an alternative entry
331 factor, and suggesting the existence of additional entry factors in the placenta.

332 The present study focused on late cohort infections from mothers who tested
333 positive at the time of delivery. It will be important to study the impact of early cohort
334 infections in mothers who are serologically positive at delivery but negative for viral
335 RNA, as infection during the first and second trimester may affect placental
336 development and morphogenesis and result in different placental pathologies and
337 clinical outcomes for mother and fetus.

338 **Materials and Methods**

339 **Cell Lines**

340 Vero E6 (African green monkey [Chlorocebus aethiops] kidney) were obtained from
341 ATCC (<https://www.atcc.org/>). Vero E6 and A549 (adenocarcinomic human alveolar
342 basal epithelial cell line)-ACE2 cells were cultured in Dulbecco's Modified Eagle
343 Medium (DMEM) supplemented with 10% fetal bovine serum (FBS) and 100 U/mL
344 penicillin and 100 µg/mL streptomycin, and maintained at 37°C with 5% CO₂.

345

346 **SARS-CoV-2 propagation and infection**

347 SARS-CoV-2 isolate USA-WA1/2020 (NR-52281) was provided by the Center for
348 Disease Control and Prevention (CDC) and obtained through BEI Resources, NIAID,
349 NIH. SARS-CoV-2 was propagated in Vero E6 cells in DMEM supplemented with 2%
350 FBS, 4.5 g/L D-glucose, 4 mM L-glutamine, 10 mM Non-essential amino acids, 1 mM
351 sodium pyruvate and 10 mM HEPES using a passage-2 stock of virus. Three days after
352 infection, supernatant containing propagated virus was filtered through an Amicon Ultra
353 15 (100 kDa) centrifugal filter (Millipore Sigma) at ~4000 rpm for 20 minutes. Flow-
354 through was discarded and virus was resuspended in DMEM supplemented as
355 described above. Infectious titers of SARS-CoV-2 were determined by plaque assay in
356 Vero E6 cells in Minimum Essential Media supplemented with 2% FBS, 4 mM L-
357 glutamine, 0.2% BSA, 10 mM HEPES and 0.12% NaHCO₃ and 0.7% agar. All MOI
358 values were based on titer determined from plaque assays on Vero E6 cells. All work
359 involving live SARS-CoV-2 was performed in the CDC/USDA-approved biosafety level-3

360 (BSL-3) facility of the Icahn School of Medicine at Mount Sinai in accordance with
361 institutional biosafety requirements.

362

363 **Placental Samples**

364 Placental tissues from SARS-CoV-2 positive women and controls were obtained at
365 delivery at Weill Cornell-NY Presbyterian by the Department of Pathology and
366 Laboratory Medicine at Weill Cornell Medicine. All women admitted for delivery were
367 tested by nasal swabs for acute SARS-CoV-2 infection by qRT-PCR, and serologically
368 for previous infection at Weill Cornell Medicine Department of Pathology and Laboratory
369 Medicine. Infants were tested for SARS-CoV-2 at birth and 1 week of age by nasal
370 swabs and RT-PCR. Placental samples were fixed for 48 hours in formalin and then
371 processed and embedded into formalin fixed paraffin embedded (FFPE) blocks by the
372 pathology department. FFPE placenta samples from 5 healthy women who tested
373 negative for SARS-CoV-2 served as controls. An additional 5 FFPE placental samples
374 with inflammation pathologies, obtained from SARS-CoV-2 negative patients, were also
375 included in the study. Unstained sections and H&E sections of the FFPE blocks were
376 performed at the Weill Cornell Clinical & Translational Science Center (CTSC) core
377 facility. Additional H&E staining was performed by the Weill Cornell Histology core
378 facility.

379

380 **SARS-CoV-2 Detection in RNA from FFPE Placental Sections by qRT-PCR**

381 Total RNA samples were prepared from FFPE placental tissue sections, followed by
382 DNaseI treatment using manufacturer's instructions (Qiagen RNeasy FFPE kit Cat#

383 73604). To quantify viral replication, as measured by the expression of nucleocapsid
384 sub genomic viral RNA along with the housekeeping gene GAPDH, two-step RT-qPCR
385 was performed using LunaScript® RT SuperMix Kit (E3010L) for cDNA synthesis and
386 Luna® Universal qPCR Master Mix (NEB #M3003) for RT-qPCR. Quantitative real-time
387 PCR reactions were performed on CFX384 Touch Real-Time PCR Detection System
388 (BioRad). The sequences of primers/probes are provided below.
389 SARS-CoV-2-N
390 Forward 5' CTCTTGTAGATCTGTTCTCTAAACGAAC 3'
391 Reverse 5' GGTCCACCAACGTAATGCG 3'
392 GAPDH
393 Forward 5' CATCACCATCTTCCAGGAGCGAGAT 3'
394 Reverse 5' GAGGCATTGCTGATGATCTTGAGGC 3'
395 qRT-PCR graphs were generated using GraphPad Prism software.
396

397 **RNA *In Situ* Hybridization to Detect SARS-CoV2 RNA on FFPE Placental Sections**
398 **Probe design.** Probes were designed with a 20-25 nucleotides homology to SARS-
399 CoV-2 genomic RNA and were assessed by NCBI BLAST to exclude off target binding
400 to other cellular transcripts. IDT OligoAnalyzer (Integrated DNA Technologies) was used
401 to identify probe pairs with similar thermodynamic properties, melting temperature 45-
402 60°C, GC content of 40-55%, and low self-complementary. The 3' end of each one of
403 the probes used for proximity ligation signal amplification is designed with a partially
404 complementary sequence to the 61bp long backbone and partially to the 21bp insert as
405 described previously (Yang et al. 2020).

406 **Tissue viral RNA staining pretreatment.** Sections of FFPE placental samples
407 were deparaffinized using 100% xylenes, 5 min at room temperature, repeated twice.
408 Slides were rinsed in 100% ethanol, 1 min at room temperature, twice and air dried.
409 Endogenous peroxidase activity was quenched by treating the samples with 0.3%
410 hydrogen peroxide, 10 min at room temperature followed by washing with DEPC treated
411 water. Samples were incubated 15 min at 95-100 °C in antigen retrieval solution
412 (ACDBio, Newark, CA, USA) rinsed in DEPC treated water and dehydrated in 100%
413 ethanol, 3 min at room temperature and air dried. Tissue sections were permeabilized
414 30 min at 40°C using RNAscope protease plus solution (ACDBio, Newark, CA, USA)
415 and rinsed in DEPC treated water.

416 **SARS-CoV-2 RNA detection by probes proximity ligation.** Hybridization was
417 performed overnight at 40°C in a buffer based on DEPC-treated water containing 2×
418 SSC, 20% formamide (Thermo Fischer Scientific, Waltham, MA, USA), 2.5 % (vol/vol)
419 polyvinylsulfonic acid, 20 mM ribonucleoside vanadyl complex (New England Biolabs,
420 Ipswich, MA, USA), 40 U/ml RNasin (Promega, Madison, WI, USA), 0.1% (vol/vol)
421 Tween 20 (Sigma Aldrich), 100 µg/ml salmon sperm DNA (Thermo Fisher Scientific,
422 Waltham, MA, USA), 100 µg/ml yeast RNA (Thermo Fisher Scientific, Waltham, MA,
423 USA). DNA probes dissolved in DEPC-treated water were added at a final concentration
424 of 100nM (Integrated DNA Technologies, Coralville, IA, USA). Samples were washed
425 briefly and incubated in 2× SSC, 20% formamide, 40 U/ml RNasin at 40 °C and then
426 washed four times (5 min each) in PBS, 0.1% (vol/vol) Tween 20, and 4 U/ml RNasin
427 (Promega, Madison, WI, USA). Slides were then incubated with 100 nM
428 insert/backbone oligonucleotides in PBS, 1× SSC, 0.1% (vol/vol) Tween 20, 100 µg/ml

429 salmon sperm DNA (Thermo Fisher Scientific, Waltham, MA, USA), 100 µg/ml yeast
430 RNA (Thermo Fisher Scientific, Waltham, MA, USA), 40 U/ml RNasin at 37 °C. After
431 four washes, tissues were incubated at 37°C with 0.1 U/µl T4 DNA ligase (New England
432 Biolabs, Ipswich, MA, USA) in 50mM Tris-HCl, 10mM MgCl₂, 1mM ATP, 1mM DTT,
433 250µg/ml BSA, 0.05% Tween 20, 40 U/ml RNasin, followed by incubation with 0.1 U/µl
434 phi29 DNA polymerase in 50 mM Tris–HCl, 10 mM MgCl₂, 10 mM (NH₄)₂SO₄, 250µM
435 dNTPs, 1mM DTT, 0.05% Tween 20, 40 U/ml RNasin pH 7.5 at 30 °C. Slides were
436 washed and endogenous biotin was blocked using Avidin/Biotin blocking kit (Vector
437 laboratories, Burlingame, CA, USA) according to the manufacture instructions. Rolling
438 cycle amplicons were identified using a biotin labeled DNA probe at a concentration of 5
439 nM at 37 °C in PBS, 1× SSC, 0.1% Tween 20, 100 µg/ml salmon sperm DNA, 100
440 µg/ml yeast RNA, 1 hr. After washing, samples were incubated with 1:100 diluted
441 streptavidin-HRP (Thermo Fisher Scientific, Waltham, MA, USA) in PBS, 60 min at
442 room temperature followed by washing. Labeling was accomplished using EnzMet kit
443 (Nanoprobes, Yaphank, NY, USA) according to manufacture instructions. Slides were
444 further labeled with rabbit anti-cytokeratin 1:250 (Dako Z0622), overnight 4°C. After
445 washing, samples were incubated with 1:1000 with anti-rabbit alkaline phosphatase
446 antibody (1:1000, Jackson immunoresearch, Baltimore, PA, USA) and stained using
447 Fast Red substrate kit according the manufacture instructions (Abcam, Cambridge, MA,
448 USA). Hematoxylin was used for counterstaining (Vector laboratories, Burlingame, CA,
449 USA), and samples were mounted in Permount (Fischer Scientific, Waltham, MA, USA).

Proximity Ligation Probes	Sequence
SARS Cov2-1	TGA GTT GGA CGT GTG TTT TCA AAA AAA AAA ACT CAG TCG TGA

	CAC TCT T
SARS Cov2-2	AGC ACG TCG CGA ACC TGT AAA AAA AAA AGA CGC TAA TAT CGT GAC C
SARS Cov2-3	AAT GCA CTC AAG AGG GTA GCA AAA AAA AAA ACT CAG TCG TGA CAC TCT T
SARS Cov2-4	GCT TTA CCA GCA CGT GCT AGA AAA AAA AAA AGA CGC TAA TAT CGT GAC C
SARS Cov2-5	TCC AAA GGC AAT AGT GCG ACA AAA AAA AAA ACT CAG TCG TGA CAC TCT T
SARS Cov2-6	ATG GCA ACC AAC ATA AGA GAA AAA AAA AAA AGA CGC TAA TAT CGT GAC C
SARS Cov2-7	CCA GTT GAA ACT ACA AAT GGA AAA AAA AAA CTC AGT CGT GAC ACT CTT
SARS Cov2-8	ACA ACA CCT AGC TCT CTG AAG AAA AAA AAA AGA CGC TAA TAT CGT GAC C
SARS Cov2-9	GAA ACA CAC AAC AGC ATC GTA AAA AAA AAA CTC AGT CGT GAC ACT CTT
SARS Cov2-10	CAC TAG ACC TTG AGA TGC ATA AAA AAA AAA GAC GCT AAT ATC GTG ACC
SARS Cov2-11	GTC TTT CAG TAC AGG TGT TAA AAA AAA AAA CTC AGT CGT GAC ACT CTT
SARS Cov2-12	TGA GCG TTT CTG CTG CAA AAA AAA AAA AAA GAC GCT AAT ATC GTG ACC
Insert	/5Phos/ACGACTGAGTTGGTCACGAT
Backbone	/5Phos/ATTAGCGTCCAGTGAATGCGAGTCCGTCTAGGAGAGTAGTACA GCAGCCGTCAAGAGTGTGTC
Detection	/5BiosG/ACGACTGAGTTGGTCACGAT

450

451 **Placental Explants and Cluster Cultures**

452 Fresh de-identified placentas from SARS-CoV-2-negative mothers were collected
453 within 30 min to 2 hours post-delivery from Labor & Delivery at WCM/NYP. Collection of
454 placentas was performed under an approved IRB exempt protocol (#20-07022453, Weill
455 Cornell Medicine.) Tissue samples were dissected by removing the fetal chorionic plate
456 and any remaining maternal decidua tissue. Primary explant cultures (1cm x 1cm x
457 2cm) containing terminal, intermediate and stem chorionic villi were further dissected,
458 washed in ice cold 1X PBS to remove maternal blood, and plated into 48-well plastic
459 dishes in DMEM/F12 medium supplemented with 10% FBS and 100 U/mL penicillin,

460 100 µg/mL streptomycin and 0.25 µg/mL amphotericin B, as previously described
461 (Massimiani et al. 2019).

462 In addition, placental cell clusters were prepared from fresh chorionic villi tissue
463 samples by mincing with scissors and 10 blade scalpels. The minced tissue was
464 digested using 0.2 mg/mL collagenase/ 0.8U/mL dispase (Roche) and recombinant
465 DNase I (Sigma) in MACS buffer (PBS/2mM EDTA/ 0.5% bovine serum albumin (BSA))
466 at 42°C with agitation by pipetting with a 5 ml stripette. The digested tissue was filtered
467 through 100 µ filters (Corning 352360), and red blood cells (RBC) were removed using
468 RBC Lysis Buffer (Biolegend 420301). Clusters were washed once in MACS buffer,
469 examined for viability with Trypan Blue (GIBCO) and plated onto Matrigel-coated 96-
470 well dishes and µ-slide 8-well chamber slides (ibidi GmbH, Germany) at confluent
471 density in DMEM/F12 supplemented with 10% FBS and penicillin/streptomycin/
472 fungizone, and were incubated at 37°C with 5% CO₂ for 24 hours prior to infection with
473 pseudovirus to allow for attachment,

474 For infection with SARS-CoV-2, Sections of fresh chorionic villi (2g) were minced
475 with sterile scalpels, digested in Accutase (Innovative Cell Technologies) for 7 min or
476 isolated using a human umbilical cord dissociation kit (Millitenyi Biotec 130-105-737),
477 and filtrated through a 100 µm cell strainer (Falcon) to obtain cell clusters of ~50-100
478 cells. Red blood cells were lysed using RBC Lysis Buffer (Biolegend), washed with
479 PBS-0.5% BSA, and resuspended in medium (DMEM-10%FBS-1% Pen-Strep-
480 Glutamax). Cell viability was determined with Trypan blue (Gibco). Cell clusters were
481 plated on Matrigel (Corning, hESC-qualified)-coated plates at 4x10⁵/well in 24-well
482 plates or 3x10⁴/well in glass-like polymer bottom 96-well plates (CellVis).

483

484 **Infection of Ex Vivo Placental Cultures**

485 **Infection of Explants and Placental clusters with Pseudovirus.** Lentiviruses
486 encoding dual Nanoluciferase/GFP reporter lentivirus and pseudotyped by SARS-CoV-2
487 spike (S) protein (D614G) or VSV-G were prepared as previously described (Tada et al.
488 2020). The viruses were concentrated 10-fold by ultracentrifugation and titers were
489 quantified by reverse transcriptase assay. Placental explant cultures and cell clusters
490 were infected with 10 µl SARS-CoV-2 S or VSV-G pseudotyped lentivirus (Tada et al.
491 2020). To determine whether NRP1 or ACE2 facilitates the infection of placental cells,
492 placental cell clusters were pretreated for 30 min with anti-NRP1 mAb (R&D Systems,
493 AF3870) or anti-ACE2 mAb (Agilent, AG-20A-0032-C50). Infected placental clusters
494 were lysed 72 hours post-infection. Luciferase activity was measured using a Promega
495 Nano-Glo Assay Kit and read on an Envision microplate luminometer (Perkin Elmer).

496 **Infection of Placental Clusters with Live SARS-CoV-2.** Placental cell clusters
497 were infected with live SARS-CoV-2 (isolate USA-WA1/2020 (NR-52281) at an MOI of
498 0.1 and 1 or mock-infected at day-1 in culture as recently described (Yang et al. 2020).
499 At the indicated hpi, cells were washed three times with PBS. For RNA analysis cells
500 were lysed in TRIzol (Invitrogen). For immunofluorescence staining cells were fixed in
501 4% formaldehyde for 60 min at room temperature. All work involving live SARS-CoV-2
502 was performed in the CDC/USDA-approved BSL-3 facility of the Icahn School of
503 Medicine at Mount Sinai in accordance with institutional biosafety requirements.

504 **qRT-PCR for Viral Load of SARS-CoV-2 Infected Placental Clusters.** Total RNA
505 was extracted using Trizol (Thermo Fisher Scientific, Waltham, MA, USA) followed by

506 ezDNase treatment (Thermo Fisher Scientific, Waltham, MA, USA) per manufacturer's
507 instructions. To quantify viral replication, measured by the accumulation of subgenomic
508 N transcripts, one-step quantitative real-time PCR was performed using the SuperScript
509 III Platinum SYBR Green One-Step qRT-PCR Kit (Invitrogen) with primers specific for
510 TRS (listed above) and beta-actin (ACTB) as an internal reference (listed below), as
511 previously described (Yang et al. 2020). Reactions were performed on a QuantStudio 6
512 Flex Real Time PCR Instrument (Applied Biosystems). The delta-delta-cycle threshold
513 ($\Delta\Delta CT$) was determined relative to ACTB and mock-infected samples. Graphs were
514 generated using GraphPad Prism software.

Primer Name	Sequence (5'-3')
ACTB-Forward	CGTCACCAACTGGGACGACA
ACTB-Reverse	CTTCTCGCGGTTGGCCTTGG

515
516 **Immunostaining of FFPE Placental Sections and Infected Placental Cell Clusters**
517 **IHC for SARS-CoV2 and Hofbauer Cells on FFPE Slides.** Immunohistochemistry
518 (IHC) was performed on FFPE slides using ImmPRESS Reagent kit (Vector
519 laboratories, Burlingame, CA, USA). FFPE slides were dewaxed in a hybrid oven for 45
520 minutes at 55°C and then rehydrated using xylenes followed by a standard ethanol
521 gradient. Antigen retrieval was performed using sodium citrate buffer, pH 6.1 in a
522 steamer for 35 minutes. Slides were blocked using 2.5% horse serum (Vector
523 laboratories) for 1 hour at room temperature and then incubated overnight at 4°C in a
524 humid chamber with primary antibodies (SARS-CoV-2-N, GeneTex GTX635679, at
525 1:100; CD163, Novus Biologicals NBP2-48846, 1:250) diluted in 1% BSA/0.1% Triton-X
526 PBS (PBST). Slides were treated with 3% hydrogen peroxide at room temperature

527 (Sigma H1009), washed 3 times with 0.1% PBST and then incubated for 1 hour at room
528 temperature with ImmPRESS anti-rabbit peroxidase conjugated antibody (Vector
529 Laboratories, Burlingame, CA, USA). Slides were again washed 3 times with 0.1%
530 PBST with final wash in PBS prior to developing using freshly prepared DAB substrate
531 (Vector Labs SK-4100). Slides were rinsed with water and counterstained with
532 Hematoxylin (RICCA Chemical Company, Arlington, TX, USA) to mark the nuclei.
533 Stained slides were dehydrated using an increasing ethanol gradient, treated with
534 xylenes, and then mounted with Permount solution (Thermo Fisher Scientific, Waltham,
535 MA, USA). Brightfield images were acquired using a Zeiss microscope (Carl Zeiss,
536 Germany).

537 **IF Staining for Pseudovirus Infected Placental Explants/Clusters.** For
538 immunofluorescence (IF) analysis, SARS-CoV-2 GFP-pseudotyped virus infected
539 explant cultures were drop-fixed overnight in 4% paraformaldehyde (PFA) in PBS
540 containing $\text{Ca}^{2+}/\text{Mg}^{2+}$ at 4°C on a rocker 72 hours post-infection. The fixed explants
541 were then dehydrated with 30% sucrose in PBS overnight at 4°C on a rocker. Explants
542 were embedded in optimal cutting temperature compound (OCT) on dry ice. Frozen
543 blocks were sectioned on a cryomicrotome at 10 micron thickness. Explant culture
544 sections were blocked for 1 hour in 10% donkey serum (Jackson ImmunoResearch
545 labs, Westgrove, PA) in 0.1% PBST. Primary antibodies (rabbit anti-cytokeratin 1:1000
546 (Dako Z0622), sheep anti-human CD31 1:500 (BD AF806) and chicken anti-GFP
547 1:1000 (Abcam ab13970)) were diluted in 10% donkey serum-0.1% PBST and
548 incubated overnight at 4°C followed by incubation with secondary antibodies
549 (AlexaFlour647-donkey anti-rabbit, AlexaFlour594-donkey anti-sheep, and

550 AlexaFlour488-donkey anti-chicken, Jackson ImmunoResearch labs, Westgrove, PA)).
551 The clusters were then stained using 4',6-diamidino-2-phenylindole (DAPI).
552 Slides were mounted with coverslips using ProLong Gold Antifade Mountant with DAPI
553 (Thermo Fisher Scientific, Waltham, MA, USA). Fluorescence microscopy was
554 performed using a Zeiss fluorescent microscope and image analysis was done using
555 ImageJ software.

556 **Immunofluorescence Staining for SARS-CoV-2 of Infected Placental Clusters.**

557 PFA-fixed cells were blocked in 5% normal donkey serum in PBS-0.05% Triton X-0.01%
558 Saponin (PBS-TSP). Primary antibodies (SARS-CoV2-N, Genetex GTX635679, 1:200;
559 KRT7, Agilent Dako M701829-2, 1:400; PECAM1, R&D AF806, 1:1000) were incubated
560 overnight at 4degC in block, followed by incubation in secondary antibodies
561 (AlexaFluor488-donkey-anti-mouse, AlexaFluor594-donkey-anti-rabbit, AlexaFluor647-
562 donkey-anti-sheep, ThermoFisher, 1:500) in PBS-TSP, and counterstaining with DAPI
563 (Thermo Fisher Scientific, Waltham, MA, USA). Images were acquired using a Zeiss
564 LSM 800 Confocal microscope and processed using Imaris software (Bitplane).
565

566 **Acknowledgements**

567 We thank the patients, their families, and healthcare workers fighting the COVID-19
568 pandemic. This work was supported by a Weill Cornell Medicine COVID-19 Research
569 Grant (H.S., R.E.S., R.N.B. Baergen), the NCI (R01CA234614) and NIAID
570 (2R01AI107301) and NIDDK (R01DK121072) to Department of Medicine, Weill Cornell
571 Medicine (R.E.S.), NIDDK (R01DK119667, R01DK119667-02S1) to S.C. R.E.S. and
572 S.C. are supported as an Irma Hirschl Trust Research Award Scholar. LBA was
573 supported in part by NYSTEM Training grant. L.A.L. is supported by an F32 post-
574 doctoral fellowship from the National Institute of Health (1F32HD096810-01A1) and
575 Weill Cornell Medicine Research Assistance for Primary Parents Award. N.R.L was
576 supported by grants from the NIH (DA046100, AI122390 and AI120898). T.T. was
577 supported by the Vilcek/Goldfarb Fellowship Endowment Fund. We would also like to
578 acknowledge Michael D. Glendenning for his technical assistance with the IHC and the
579 WCM Histology Core.

580

581 **Competing Interests**

582 R.E.S. is on the scientific advisory board of Miromatrix Inc and is a consultant and
583 speaker for Alnylam Inc.

584

585 **References**

586 Alamar, I., M. H. Abu-Arja, T. Heyman, D. J. Roberts, N. Desai, P. Narula, and B. Dygulski.
587 2020. 'A Possible Case of Vertical Transmission of Severe Acute Respiratory Syndrome
588 Coronavirus 2 (SARS-CoV-2) in a Newborn With Positive Placental In Situ Hybridization
589 of SARS-CoV-2 RNA', *J Pediatric Infect Dis Soc*, 9: 636-39.

590 Arad, A., S. Nammouz, Y. Nov, G. Ohel, J. Bejar, and Z. Vadasz. 2017. 'The Expression of
591 Neuropilin-1 in Human Placentas From Normal and Preeclamptic Pregnancies', *Int J
592 Gynecol Pathol*, 36: 42-49.

593 Baergen, R. N., and D. S. Heller. 2020. 'Placental Pathology in Covid-19 Positive Mothers:
594 Preliminary Findings', *Pediatr Dev Pathol*, 23: 177-80.

595 Baston-Buest, D. M., A. C. Porn, A. Schanz, J. S. Kruessel, W. Janni, and A. P. Hess. 2011.
596 'Expression of the vascular endothelial growth factor receptor neuropilin-1 at the human
597 embryo-maternal interface', *Eur J Obstet Gynecol Reprod Biol*, 154: 151-6.

598 Blanco-Melo, D., B. E. Nilsson-Payant, W. C. Liu, S. Uhl, D. Hoagland, R. Møller, T. X. Jordan,
599 K. Oishi, M. Panis, D. Sachs, T. T. Wang, R. E. Schwartz, J. K. Lim, R. A. Albrecht, and
600 B. R. tenOever. 2020. 'Imbalanced Host Response to SARS-CoV-2 Drives Development
601 of COVID-19', *Cell*, 181: 1036-45.e9.

602 Burton, G. J., A. L. Fowden, and K. L. Thornburg. 2016. 'Placental Origins of Chronic Disease',
603 *Physiol Rev*, 96: 1509-65.

604 Cantuti-Castelvetri, L., R. Ojha, L. D. Pedro, M. Djannatian, J. Franz, S. Kuivanen, F. van der
605 Meer, K. Kallio, T. Kaya, M. Anastasina, T. Smura, L. Levanov, L. Szirovicza, A. Tobi, H.
606 Kallio-Kokko, P. Österlund, M. Joensuu, F. A. Meunier, S. J. Butcher, M. S. Winkler, B.
607 Mollenhauer, A. Helenius, O. Gokce, T. Teesalu, J. Hepojoki, O. Vapalahti, C.
608 Stadelmann, G. Balistreri, and M. Simons. 2020. 'Neuropilin-1 facilitates SARS-CoV-2
609 cell entry and infectivity', *Science*, 370: 856-60.

610 Daly, J. L., B. Simonetti, K. Klein, K. E. Chen, M. K. Williamson, C. Antón-Plágaro, D. K.
611 Shoemark, L. Simón-Gracia, M. Bauer, R. Hollandi, U. F. Greber, P. Horvath, R. B.
612 Sessions, A. Helenius, J. A. Hiscox, T. Teesalu, D. A. Matthews, A. D. Davidson, B. M.
613 Collins, P. J. Cullen, and Y. Yamauchi. 2020. 'Neuropilin-1 is a host factor for SARS-
614 CoV-2 infection', *Science*, 370: 861-65.

615 Daniloski, Z., T. X. Jordan, H. H. Wessels, D. A. Hoagland, S. Kasela, M. Legut, S. Maniatis, E.
616 P. Mimitou, L. Lu, E. Geller, O. Danziger, B. R. Rosenberg, H. Phatnani, P. Smibert, T.
617 Lappalainen, B. R. tenOever, and N. E. Sanjana. 2021. 'Identification of Required Host
618 Factors for SARS-CoV-2 Infection in Human Cells', *Cell*, 184: 92-105.e16.

619 Debelenko, L., I. Katsyv, A. M. Chong, L. Peruyero, M. Szabolcs, and A. C. Uhlemann. 2021.
620 'Trophoblast damage with acute and chronic intervillousis: disruption of the placental
621 barrier by severe acute respiratory syndrome coronavirus 2', *Hum Pathol*, 109: 69-79.

622 Della Gatta, A. N., R. Rizzo, G. Pilu, and G. Simonazzi. 2020. 'Coronavirus disease 2019 during
623 pregnancy: a systematic review of reported cases', *Am J Obstet Gynecol*, 223: 36-41.

624 Edlow, A. G., J. Z. Li, A. Y. Collier, C. Atyeo, K. E. James, A. A. Boatman, K. J. Gray, E. A. Bordt,
625 L. L. Shook, L. M. Yonker, A. Fasano, K. Diouf, N. Croul, S. Devane, L. J. Yockey, R.
626 Lima, J. Shui, J. D. Matute, P. H. Lerou, B. O. Akinwunmi, A. Schmidt, J. Feldman, B. M.
627 Hauser, T. M. Caradonna, D. De la Flor, P. D'Avino, J. Regan, H. Corry, K. Coxen, J.
628 Fajnzylber, D. Pepin, M. S. Seaman, D. H. Barouch, B. D. Walker, X. G. Yu, A. J.
629 Kaimal, D. J. Roberts, and G. Alter. 2020. 'Assessment of Maternal and Neonatal SARS-
630 CoV-2 Viral Load, Transplacental Antibody Transfer, and Placental Pathology in
631 Pregnancies During the COVID-19 Pandemic', *JAMA Netw Open*, 3: e2030455.

632 Facchetti, F., M. Bugatti, E. Drera, C. Tripodo, E. Sartori, V. Cancila, M. Papaccio, R. Castellani,
633 S. Casola, M. B. Boniotti, P. Cavadini, and A. Lavazza. 2020. 'SARS-CoV2 vertical
634 transmission with adverse effects on the newborn revealed through integrated
635 immunohistochemical, electron microscopy and molecular analyses of Placenta',
636 *EBioMedicine*, 59: 102951.

637 Garrido-Pontnou, M., A. Navarro, J. Camacho, F. Crispi, M. Alguacil-Guillén, A. Moreno-Baró, J.
638 Hernandez-Losa, M. Sesé, Y. Cajal S. Ramón, I. Garcia Ruiz, B. Serrano, P. Garcia-
639 Aguilar, A. Suy, J. C. Ferreres, and A. Nadal. 2021. 'Diffuse trophoblast damage is the
640 hallmark of SARS-CoV-2-associated fetal demise', *Mod Pathol*: 1-6.

641 Hecht, J. L., B. Quade, V. Deshpande, M. Mino-Kenudson, D. T. Ting, N. Desai, B. Dugulsa, T.
642 Heyman, C. Salafia, D. Shen, S. V. Bates, and D. J. Roberts. 2020a. 'SARS-CoV-2 can
643 infect the placenta and is not associated with specific placental histopathology: a series
644 of 19 placentas from COVID-19-positive mothers', *Mod Pathol*: 1-12.

645 Hoffmann, M., H. Kleine-Weber, S. Schroeder, N. Krüger, T. Herrler, S. Erichsen, T. S.
646 Schiergens, G. Herrler, N. H. Wu, A. Nitsche, M. A. Müller, C. Drosten, and S.
647 Pöhlmann. 2020. 'SARS-CoV-2 Cell Entry Depends on ACE2 and TMPRSS2 and Is
648 Blocked by a Clinically Proven Protease Inhibitor', *Cell*, 181: 271-80.e8.

649 Hosier, H., S. F. Farhadian, R. A. Morotti, U. Deshmukh, A. Lu-Culligan, K. H. Campbell, Y.
650 Yasumoto, C. B. Vogels, A. Casanovas-Massana, P. Vijayakumar, B. Geng, C. D. Odio,
651 J. Fournier, A. F. Brito, J. R. Fauver, F. Liu, T. Alpert, R. Tal, K. Szigeti-Buck, S.
652 Perincheri, C. Larsen, A. M. Gariepy, G. Aguilar, K. L. Fardelmann, M. Harigopal, H. S.

653 Taylor, C. M. Pettker, A. L. Wyllie, C. D. Cruz, A. M. Ring, N. D. Grubaugh, A. I. Ko, T. L.
654 Horvath, A. Iwasaki, U. M. Reddy, and H. S. Lipkind. 2020. 'SARS-CoV-2 infection of the
655 placenta', *J Clin Invest*, 130: 4947-53.

656 John, R., and M. Hemberger. 2012. 'A placenta for life', *Reprod Biomed Online*, 25: 5-11.

657 Kimberlin, D. W., and S. Stagno. 2020. 'Can SARS-CoV-2 Infection Be Acquired In Utero?:
658 More Definitive Evidence Is Needed', *JAMA*.

659 Li, M., L. Chen, J. Zhang, C. Xiong, and X. Li. 2020. 'The SARS-CoV-2 receptor ACE2
660 expression of maternal-fetal interface and fetal organs by single-cell transcriptome
661 study', *PLoS One*, 15: e0230295.

662 Lu-Culligan, A., A. R. Chavan, P. Vijayakumar, L. Irshaid, E. M. Courchaine, K. M. Milano, Z.
663 Tang, S. D. Pope, E. Song, C. B. F. Vogels, W. J. Lu-Culligan, K. H. Campbell, A.
664 Casanovas-Massana, S. Bermejo, J. M. Toothaker, H. J. Lee, F. Liu, W. Schulz, J.
665 Fournier, M. C. Muenker, A. J. Moore, L. Konnikova, K. M. Neugebauer, A. Ring, N. D.
666 Grubaugh, A. I. Ko, R. Morotti, S. Guller, H. J. Kliman, A. Iwasaki, and S. F. Farhadian.
667 2021. 'Maternal respiratory SARS-CoV-2 infection in pregnancy is associated with a
668 robust inflammatory response at the maternal-fetal interface', *Med (N Y)*, 2: 591-
669 610.e10.

670 Maltepe, E., A. I. Bakardjiev, and S. J. Fisher. 2010. 'The placenta: transcriptional, epigenetic,
671 and physiological integration during development', *J Clin Invest*, 120: 1016-25.

672 Marín Gabriel, M. A., M. Reyne Vergeli, S. Caserío Carbonero, L. Sole, T. Carrizosa Molina, I.
673 Rivero Calle, I. Cuadrado Pérez, B. Álvarez Fernández, A. Forti Buratti, and A.
674 Fernández-Cañadas Morillo. 2020. 'Maternal, Perinatal and Neonatal Outcomes With
675 COVID-19: A Multicenter Study of 242 Pregnancies and Their 248 Infant Newborns
676 During Their First Month of Life', *Pediatr Infect Dis J*, 39: e393-e97.

677 Massimiani, M., L. A. Lacko, C. S. Burke Swanson, S. Salvi, L. B. Argueta, S. Moresi, S.
678 Ferrazzani, S. E. Gelber, R. N. Baergen, N. Toschi, L. Campagnolo, and H. Stuhlmann.
679 2019. 'Increased circulating levels of Epidermal Growth Factor-like Domain 7 in pregnant
680 women affected by preeclampsia', *Transl Res*, 207: 19-29.

681 Morotti, D., M. Cadamuro, E. Rigoli, A. Sonzogni, A. Gianatti, C. Parolin, L. Patanè, and D. A.
682 Schwartz. 2021. 'Molecular Pathology Analysis of SARS-CoV-2 in Syncytiotrophoblast
683 and Hofbauer Cells in Placenta from a Pregnant Woman and Fetus with COVID-19',
684 *Pathogens*, 10.

685 Mullins, E., M. L. Hudak, J. Banerjee, T. Getzlaff, J. Townson, K. Barnette, R. Playle, A. Perry,
686 T. Bourne, and C. C. Lees. 2021. 'Pregnancy and neonatal outcomes of COVID-19:

687 coreporting of common outcomes from PAN-COVID and AAP-SONPM registries',
688 *Ultrasound Obstet Gynecol*, 57: 573-81.

689 Mulvey, J. J., C. M. Magro, L. X. Ma, G. J. Nuovo, and R. N. Baergen. 2020. 'Analysis of
690 complement deposition and viral RNA in placentas of COVID-19 patients', *Ann Diagn
691 Pathol*, 46: 151530.

692 Ou, X., Y. Liu, X. Lei, P. Li, D. Mi, L. Ren, L. Guo, R. Guo, T. Chen, J. Hu, Z. Xiang, Z. Mu, X.
693 Chen, J. Chen, K. Hu, Q. Jin, J. Wang, and Z. Qian. 2020. 'Characterization of spike
694 glycoprotein of SARS-CoV-2 on virus entry and its immune cross-reactivity with SARS-
695 CoV', *Nat Commun*, 11: 1620.

696 Ouyang, Y., T. Bagalkot, W. Fitzgerald, E. Sadovsky, T. Chu, A. Martínez-Marchal, M. Brieño-
697 Enríquez, E. J. Su, L. Margolis, A. Sorkin, and Y. Sadovsky. 2021. 'Term Human
698 Placental Trophoblasts Express SARS-CoV-2 Entry Factors ACE2, TMPRSS2, and
699 Furin', *mSphere*, 6.

700 Penfield, C. A., S. G. Brubaker, M. A. Limaye, J. Lighter, A. J. Ratner, K. M. Thomas, J. A.
701 Meyer, and A. S. Roman. 2020. 'Detection of severe acute respiratory syndrome
702 coronavirus 2 in placental and fetal membrane samples', *Am J Obstet Gynecol MFM*, 2:
703 100133.

704 Pique-Regi, R., R. Romero, A. L. Tarca, F. Luca, Y. Xu, A. Alazizi, Y. Leng, C. D. Hsu, and N.
705 Gomez-Lopez. 2020. 'Does the human placenta express the canonical cell entry
706 mediators for SARS-CoV-2?', *Elife*, 9.

707 Prabhu, M., K. Cagino, K. C. Matthews, R. L. Friedlander, S. M. Glynn, J. M. Kubiak, Y. J. Yang,
708 Z. Zhao, R. N. Baergen, J. I. DiPace, A. S. Razavi, D. W. Skupski, J. R. Snyder, H. K.
709 Singh, R. B. Kalish, C. M. Oxford, and L. E. Riley. 2020. 'Pregnancy and postpartum
710 outcomes in a universally tested population for SARS-CoV-2 in New York City: a
711 prospective cohort study', *BJOG*, 127: 1548-56.

712 Rossant, J., and J. C. Cross. 2001. 'Placental development: lessons from mouse mutants', *Nat
713 Rev Genet*, 2: 538-48.

714 Salvatore, C. M., J. Y. Han, K. P. Acker, P. Tiwari, J. Jin, M. Brandler, C. Cangemi, L. Gordon,
715 A. Parow, J. DiPace, and P. DeLaMora. 2020. 'Neonatal management and outcomes
716 during the COVID-19 pandemic: an observation cohort study', *Lancet Child Adolesc
717 Health*, 4: 721-27.

718 Schneider, W. M., J. M. Luna, H. H. Hoffmann, F. J. Sánchez-Rivera, A. A. Leal, A. W.
719 Ashbrook, J. Le Pen, I. Ricardo-Lax, E. Michailidis, A. Peace, A. F. Stenzel, S. W. Lowe,

720 M. R. MacDonald, C. M. Rice, and J. T. Poirier. 2021. 'Genome-Scale Identification of
721 SARS-CoV-2 and Pan-coronavirus Host Factor Networks', *Cell*, 184: 120-32.e14.

722 Schwartz, D. A. 2020. 'An Analysis of 38 Pregnant Women with COVID-19, Their Newborn
723 Infants, and Maternal-Fetal Transmission of SARS-CoV-2: Maternal Coronavirus
724 Infections and Pregnancy Outcomes', *Arch Pathol Lab Med*.

725 Schwartz, D. A., M. Baldewijns, A. Benachi, M. Bugatti, R. R. J. Collins, D. De Luca, F.
726 Facchetti, R. L. Linn, L. Marcelis, D. Morotti, R. Morotti, W. T. Parks, L. Patanè, S.
727 Prevot, B. Pulinx, V. Rajaram, D. Strybol, K. Thomas, and A. J. Vivanti. 2021. 'Chronic
728 Histiocytic Intervillitis With Trophoblast Necrosis Is a Risk Factor Associated With
729 Placental Infection From Coronavirus Disease 2019 (COVID-19) and Intrauterine
730 Maternal-Fetal Severe Acute Respiratory Syndrome Coronavirus 2 (SARS-CoV-2)
731 Transmission in Live-Born and Stillborn Infants', *Arch Pathol Lab Med*, 145: 517-28.

732 Shanes, E. D., L. B. Mithal, S. Otero, H. A. Azad, E. S. Miller, and J. A. Goldstein. 2020.
733 'Placental Pathology in COVID-19', *Am J Clin Pathol*, 154: 23-32.

734 Shang, J., Y. Wan, C. Luo, G. Ye, Q. Geng, A. Auerbach, and F. Li. 2020. 'Cell entry
735 mechanisms of SARS-CoV-2', *Proc Natl Acad Sci U S A*.

736 Singh, M., V. Bansal, and C. Feschotte. 2020. 'A Single-Cell RNA Expression Map of Human
737 Coronavirus Entry Factors', *Cell Rep*, 32: 108175.

738 Tada, T., C. Fan, J. S. Chen, R. Kaur, K. A. Stapleford, H. Gristick, B. M. Dcosta, C. B. Wilen,
739 C. M. Nirmigean, and N. R. Landau. 2020. 'An ACE2 Microbody Containing a Single
740 Immunoglobulin Fc Domain Is a Potent Inhibitor of SARS-CoV-2', *Cell Rep*, 33: 108528.

741 Taglauer, E., Y. Benarroch, K. Rop, E. Barnett, V. Sabharwal, C. Yarrington, and E. M.
742 Wachman. 2020. 'Consistent localization of SARS-CoV-2 spike glycoprotein and ACE2
743 over TMPRSS2 predominance in placental villi of 15 COVID-19 positive maternal-fetal
744 dyads', *Placenta*, 100: 69-74.

745 Verma, S., C. S. Joshi, R. B. Silverstein, M. He, E. B. Carter, and I. U. Mysorekar. 2021. 'SARS-
746 CoV-2 colonization of maternal and fetal cells of the human placenta promotes alteration
747 of local renin-angiotensin system', *Med (N Y)*, 2: 575-90.e5.

748 Vivanti, A. J., C. Vauloup-Fellous, S. Prevot, V. Zupan, C. Suffee, J. Do Cao, A. Benachi, and D.
749 De Luca. 2020. 'Transplacental transmission of SARS-CoV-2 infection', *Nat Commun*,
750 11: 3572.

751 Wang, R., C. R. Simoneau, J. Kulsuptrakul, M. Bouhaddou, K. A. Travisano, J. M. Hayashi, J.
752 Carlson-Steivermer, J. R. Zengel, C. M. Richards, P. Fozouni, J. Oki, L. Rodriguez, B.
753 Joehnk, K. Walcott, K. Holden, A. Sil, J. E. Carette, N. J. Krogan, M. Ott, and A. S.

754 Puschnik. 2021. 'Genetic Screens Identify Host Factors for SARS-CoV-2 and Common
755 Cold Coronaviruses', *Cell*, 184: 106-19.e14.

756 Wei, J., M. M. Alfajaro, P. C. DeWeirdt, R. E. Hanna, W. J. Lu-Culligan, W. L. Cai, M. S. Strine,
757 S. M. Zhang, V. R. Graziano, C. O. Schmitz, J. S. Chen, M. C. Mankowski, R. B. Filler,
758 N. G. Ravindra, V. Gasque, F. J. de Miguel, A. Patil, H. Chen, K. Y. Oguntuyo, L.
759 Abriola, Y. V. Surovtseva, R. C. Orchard, B. Lee, B. D. Lindenbach, K. Polit, D. van Dijk,
760 C. Kadoch, M. D. Simon, Q. Yan, J. G. Doench, and C. B. Wilen. 2021. 'Genome-wide
761 CRISPR Screens Reveal Host Factors Critical for SARS-CoV-2 Infection', *Cell*, 184: 76-
762 91.e13.

763 Woodworth, K. R., E. O. Olsen, V. Neelam, E. L. Lewis, R. R. Galang, T. Oduyebo, K. Aveni, M.
764 M. Yazdy, E. Harvey, N. D. Longcore, J. Barton, C. Fussman, S. Siebman, M. Lush, P.
765 H. Patrick, U. A. Halai, M. Valencia-Prado, L. Orkis, S. Sowunmi, L. Schlosser, S.
766 Khuwaja, J. S. Read, A. J. Hall, D. Meaney-Delman, S. R. Ellington, S. M. Gilboa, and V.
767 T. Tong. 2020. 'Birth and Infant Outcomes Following Laboratory-Confirmed SARS-CoV-2
768 Infection in Pregnancy - SET-NET, 16 Jurisdictions, March 29-October 14, 2020',
769 *MMWR Morb Mortal Wkly Rep*, 69: 1635-40.

770 Yang, L., Y. Han, B. E. Nilsson-Payant, V. Gupta, P. Wang, X. Duan, X. Tang, J. Zhu, Z. Zhao,
771 F. Jaffré, T. Zhang, T. W. Kim, O. Harschnitz, D. Redmond, S. Houghton, C. Liu, A. Naji,
772 G. Ciceri, S. Guttikonda, Y. Bram, D. T. Nguyen, M. Cioffi, V. Chandar, D. A. Hoagland,
773 Y. Huang, J. Xiang, H. Wang, D. Lyden, A. Borczuk, H. J. Chen, L. Studer, F. C. Pan, D.
774 D. Ho, B. R. tenOever, T. Evans, R. E. Schwartz, and S. Chen. 2020. 'A Human
775 Pluripotent Stem Cell-based Platform to Study SARS-CoV-2 Tropism and Model Virus
776 Infection in Human Cells and Organoids', *Cell Stem Cell*, 27: 125-36.e7.

777 Zambrano, L. D., S. Ellington, P. Strid, R. R. Galang, T. Oduyebo, V. T. Tong, K. R. Woodworth,
778 J. F. Nahabedian, 3rd, E. Azziz-Baumgartner, S. M. Gilboa, and D. Meaney-Delman.
779 2020. 'Update: Characteristics of Symptomatic Women of Reproductive Age with
780 Laboratory-Confirmed SARS-CoV-2 Infection by Pregnancy Status - United States,
781 January 22-October 3, 2020', *MMWR Morb Mortal Wkly Rep*, 69: 1641-47.

782

783

784 **Figure legends**

785 **Figure 1. SARS-CoV-2 virus is present in placentas from infected mothers and results in**
786 **inflammatory responses.** (A) Graph showing $\Delta\Delta CT$ values of RNA samples isolated from
787 FFPE patient placenta slides from the different cohorts. A student's t-test comparing the 3
788 positive cohorts (High Positive, Positive, Borderline Positive) to the negative control cohort
789 resulted in statistically significant higher viral load in the High Positive and Positive cohorts (***
790 = p-value < 0.001). (B) Brightfield microscopy images of a representative COVID High positive
791 patient (P3) and a representative negative control patient sample (C1). Slides were stained by
792 H&E, *in situ* PLAYR for SARS-CoV2-RNA counterstained for syncytial trophoblast marker
793 cytokeratin (KRT7, red), and by immunohistochemistry for SARS-CoV2-N protein (brown) as
794 well as for CD163+ Hofbauer cells (HBC). Scale bars = 100 μ m.

795

796 **Figure 2. Placental explant and cell clusters can be infected by SARS-CoV-2 S**
797 **protein pseudotyped lentivirus and infection can be blocked by anti-ACE2 and anti-NRP1**
798 **antibodies.** (A) Graphs showing relative luminescence units (RLU) from infected explant
799 cultures 72 hpi with the addition of reverse transcriptase inhibitor, Nevirapine (NVP). (B) Graphs
800 showing RLU from infected isolated primary placental clusters 72 hpi with the addition of
801 blocking antibodies against ACE2, NRP1. Statistical analysis was performed using one-way
802 Anova (** = p-value < 0.005, *** = p-value < 0.001). (C) Brightfield and live fluorescence
803 microscopy images of cultured placental explants Mock (left column), or 72hpi with either Lenti-
804 SARS-CoV2-S Pseudovirus (center column) or Lenti-VSV-G (right column). (D) Fluorescence
805 microscopy on mock (top row) and Lenti-SARS-CoV2-S infected (center row) or Lenti-VSV-G
806 infected (bottom row) explant sections stained for the GFP reporter (green) syncytial trophoblast
807 marker, cytokeratin (KRT7, grey), endothelial marker CD31 (red) and DAPI nuclear stain (blue).
808 Scale bars = 500 μ m.

809

810 **Figure 3. Primary human placenta cells can be infected with SARS-CoV-2 *ex***
811 ***vivo*.** (A) qRT-PCR analysis of relative viral N subgenomic RNA expression in primary placental
812 cell clusters infected with SARS-CoV-2 *ex vivo* (MOI=1) for 24 hours and normalized to ACTB
813 levels. (mean+/- SD; n=12 from 4 repeated experiments; ****p<0.0001) . (B) Three-dimensional
814 reconstruction of confocal imaging of primary placental cell clusters infected with SARS-CoV-
815 2 *ex vivo* (MOI=1) at 24hpi, stained for trophoblast marker KRT7 (green), SARS-N (red),
816 endothelial marker CD31 (grey), and DAPI (blue). Scale bar = 30 μ m. (C) Confocal imaging of
817 primary placental cell clusters infected with MOCK (top rows) or SARS-CoV-2 (MOI=1, bottom
818 rows) *ex vivo* at 24hpi, stained for trophoblast marker KRT7 (green), SARS-N (red), endothelial
819 marker CD31 (grey), and DAPI (blue). Arrows indicate presence of SARS-N nucleocapsid
820 protein in trophoblast and endothelial cells. Scale bar = 20 μ m.

821

822 **Table 1. Clinical presentations of SARS-CoV-2 positive mothers, fetal outcomes and placental**
823 **pathologies.**

824 Overview of 65 Patients included in study. 55 COVID-positive, 10 COVID-negative.

825 Abbreviations: FVM: Fetal Vascular Malperfusion, MVM: Maternal Vascular Malperfusion, DFM:

826 Decreased Fetal Movement, MCI: Massive Chronic Intervillitis, MFI: Maternal Floor Infarction,

827 CHI: Chronic Histiocytic Intervillitis, IUFD: Intra-Uterine Fetal Demise, T2D: Type 2 Diabetes,

828 Mec: Meconium, IVT: Intervillous Thrombi, VUE: Villitis of Unknown Etiology/Chronic

829 Villitis, ACA: Acute Chorioamnitis, IAI: Intra-Amniotic Infection/Chorioamnitis, HTN:

830 Hypertension, IUGR: Intra-Uterine Growth Restriction, GDM: Gestational Diabetes Mellitus,

831 PPROM: Preterm Premature Rupture of Membranes, PTL: Preterm Labor, PAPP-A: Pregnancy-

832 associated Plasma Protein A, UCTD: Undifferentiated Connective Tissue Disorder, HCV:

833 Hepatitis C Virus, ITP: Immune Thrombocytopenic Purpura. IUGR: intrauterine growth

834 restriction. ICP: intrahepatic cholestasis of pregnancy. Gray Shaded Rows = Fetal Demise/NICU

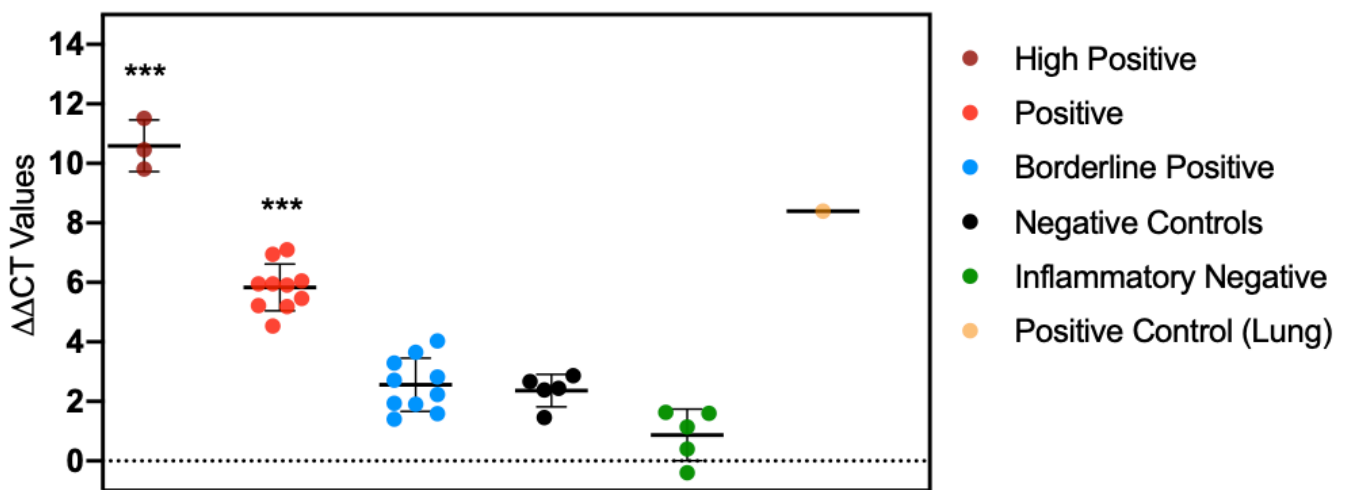
835 admission.

Table 1

	Mother Clinical Presentation				Fetal Outcome			Pregnancy Pathologies			Placenta Viral RNA		
	Case	Mat Age	Gest Age	Mother COVID +/-	Patient History		Birth weight	Apgar 1 min	Apgar 5 min	FVM	MVM	Other pathology	
High Positive	P1	35	25	+	Symptomatic COVID-19, DFM, Delivered due to nonreassuring fetal status		650	1	8	-	-	MCI	+
	P2	29	36	+	Symptomatic COVID-19		2850	9	9	-	-	-	+
	P3	34	30	+	Symptomatic COVID-19, DFM, IUFD		1389	0	0	-	-	MFI, CHI	+
	P4	29	40	+	Symptomatic COVID-19		3400	9	9	+	-	-	+
	P5	40	36	+	T2D (poorly controlled), Placenta previa		2680	9	9	-	-	-	+
	P6	16	32	+	Symptomatic COVID-19, PTL		1740	9	8	-	+		+
	P7	26	37	+	Asymptomatic COVID-19, T2D (poorly controlled), DFM, IUFD		3200	0	0	-	-	Villous Dysmaturity	+
	P8	31	39	+	Symptomatic COVID-19		3140	9	9	-	-	Mec, IVT	+
	P9	30	38	+	Symptomatic COVID-19		3910	9	9	+	-	VUE, Mec	+
	P10	41	39	+	Asymptomatic COVID-19		3770	9	9	-	-	VUE	+
	P11	28	39	+	Asymptomatic COVID-19		3300	9	9	-	-	Mec	+
	P12	34	37	+	ICP		2900	9	9	-	-	-	+
	P13	31	40	+	Asymptomatic COVID-19		3340	9	9	-	-	Mec	+
Positive	P14	30	38	+	Symptomatic COVID-19, Intrapartum chorioamnionitis		3360	9	9	+	-	Mec, Furcate cord	+
	P15	26	38	+	Asymptomatic COVID-19		3050	9	9	+	-	-	+
	P16	19	38	+	Symptomatic COVID-19		2390	9	9	+	+	ACA	+
	P17	28	40	+	Asymptomatic COVID-19		3820	9	9	+	-	Mec	+
	P18	28	41	+	Symptomatic COVID-19		4020	8	9	+	-	VUE, IDA, Mec	+
	P19	41	40	+	Symptomatic COVID-19		4115	9	9	+	-	Mec	+
	P20	32	38	+	Asymptomatic COVID-19		3160	9	9	-	-	Twisted Cord	+
	P21	26	39	+	Symptomatic COVID-19		3720	9	9	+	-	Hofbauer hyperplasia	+
	P22	20	38	+	Symptomatic COVID-19		3685	6	9	+	-	IAI, Mec	+
	P23	25	39	+	Asymptomatic COVID-19		3000	9	9	-	-	Villitis	+
Negative Samples	P24	40	39	+	Asymptomatic COVID-19		3720	9	9	+	-	-	-
	P25	40	37	+	Symptomatic COVID-19, PEC		2060	8	9	-	+	Mec	-
	P26	38	39	+	Symptomatic COVID-19, ITP, Protein S deficiency, Gestational HTN		3890	9	9	+	-	Funisitis	-
	P27	26	40	+	Chronic HTN. Symptomatic COVID-19		3799	9	9	+	-	-	-
	P28	37	39	+	Asymptomatic COVID-19. Autoimmune gastritis.		2415	9	9	-	+	-	-
	P29	40	33	+	Symptomatic COVID-19, IUGR, PEC, Delivered for nonreassuring fetal status		1690	8	8	-	+	Mec	-
	P30	33	35	+	Symptomatic COVID-19, Dichorionic twins, PEC	2280 (A) 2810 (B)	8 (A) 8 (B)	9 (A) 9 (B)	+	+	VUE	-	
	P31	23	39	+	Asymptomatic COVID-19		3580	8	9	-	-	Villitis	-
	P32	25	38	+	Asymptomatic COVID-19		3920	9	9	-	-	Mec	-
	P33	34	39	+	Symptomatic COVID-19		3360	9	9	-	-	Mec	-
	P34	40	37	+	Asymptomatic COVID-19		3400	8	9	-	-	-	-
	P35	37	41	+	Symptomatic COVID-19		3900	9	9	-	-	IAI, Mec	-
	P36	39	37	+	Asymptomatic COVID-19		2650	9	9	-	-	Villous dysmaturity	-
	P37	34	39	+	Asymptomatic COVID-19		2510	9	9	-	+	-	-
	P38	33	23	+	COVID-19 remote from delivery. Fetal anencephaly, intrapartum fetal demise		370	0	0	-	-	-	-
	P39	30	39	+	Asymptomatic COVID-19		3910	9	9	+	-	Villitis	-
	P40	31	40	+	Symptomatic COVID-19 remote from delivery		3200	8	9	-	-	-	-
	P41	30	39	+	Symptomatic COVID-19 remote from delivery		3650	9	9	+	-	Chorionic cysts, IAI, Mec	-
	P42	27	41	+	Symptomatic COVID-19, low PAPP-A, Gestational HTN		3630	8	9	-	-	Focal chorangiosis	-
	P43	23	37	+	Symptomatic COVID-19 remote from delivery		2510	9	9	-	-	IVT	-
	P44	31	36	+	ICP, Asymptomatic COVID-19		3290	9	9	-	-	IVT, Mec	-
	P45	29	37	+	Symptomatic COVID-19, low PAPP-A		2530	8	9	-	+	-	-
	P46	29	36	+	Symptomatic COVID-19		2850	9	9	-	-	-	-
	P47	40	38	+	Symptomatic COVID-19 remote from delivery		2820	9	9	-	+	-	-
	P48	32	40	+	Symptomatic COVID-19 remote from delivery		3360	9	9	-	+	VUE	-
	P49	51	37	+	Symptomatic COVID-19 remote from delivery, T2D		3080	9	10	-	-	VUE	-
	P50	41	38	+	Symptomatic COVID-19 remote from delivery, Asthma		2990	8	9	+	+	-	-
	P51	38	39	+	Symptomatic COVID-19 remote from delivery		3010	9	9	-	-	VUE, IVT	-
	P52	38	39	+	Symptomatic COVID-19 remote from delivery		3840	9	9	-	-	-	-
	P53	33	38	+	Symptomatic COVID-19, Long QT syndrome, remote from delivery		3005	9	9	-	-	-	-
	P54	38	36	+	Symptomatic COVID-19 remote from delivery, Dichorionic twins, PTL	2680 (A) 2740 (B)	9 (A) 9 (B)	9 (A) 9 (B)	-	-	-	-	
	P55	35	39	+	Symptomatic COVID-19 remote from delivery		2870	9	9	+	+	Villitis	-
Negative Controls	C1	32	40	-	Subglottic stenosis	NA	9	9	-	-	Mec	-	
	C2	29	39	-	Low PAPP-A, UCTD, celiac disease	3470	9	9	-	-	Mec	-	
	C3	39	34	-	PPROM	2320	9	9	-	-	IVT	-	
	C4	31	40	-	COVID-19 in first trimester	3392	9	9	-	-	IVT	-	
	C5	36	39	-	Gestational HTN, GDM	3277	9	9	-	-	ACA	-	
Inflammatory Samples	I1	32	38	-	Intrapartum chorioamnionitis	3145	9	9	-	-	ACA, Acute funisitis, Mec	-	
	I2	28	40	-	No medical history	3100	9	9	-	-	VUE, ACA	-	
	I3	33	38	-	Opioid use disorder, HCV, Placental abruption	2664	9	9	+	-	VUE, Acute funisitis	-	
	I4	42	38	-	Gestational HTN, GDM	2891	9	9	-	-	ACA, Acute funisitis	-	
	I5	34	39	-	ITP	3447	7	9	-	+	ACA, Acute funisitis, Mec	-	

Figure 1

A



B

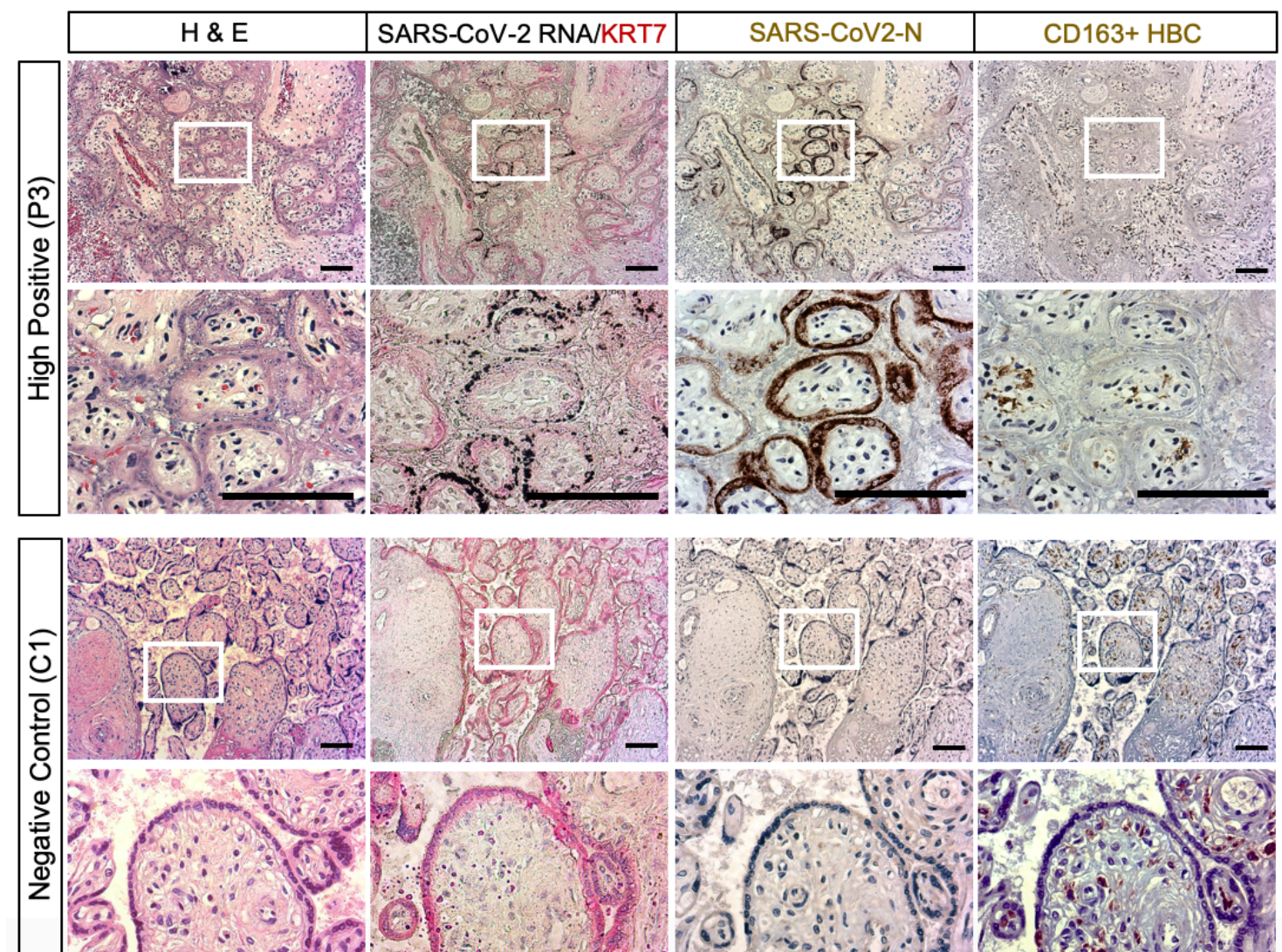


Figure 2

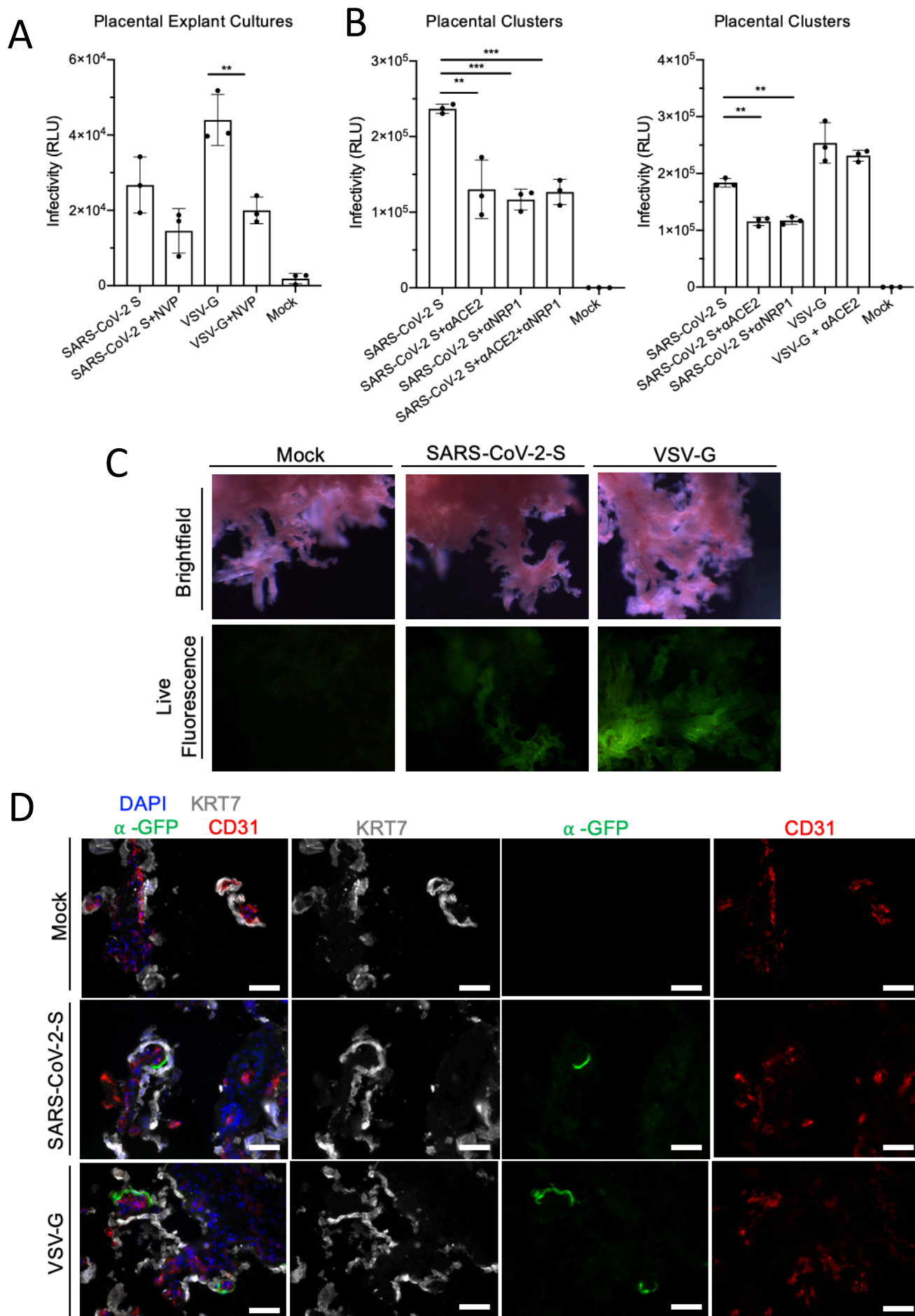


Figure 3

